Microchimica Acta (2019) 186:807
https://doi.org/10.1007/s00604-019-3915-6

ORIGINAL PAPER

Carbon fibers coated with urchin-like copper sulfide for nonenzymatic voltammetric sensing of glucose

Murugan Keerthi[1] · Bhuvanenthiran Mutharani[1] · Shen-Ming Chen[1] · Palraj Ranganathan[2]

Received: 30 May 2019 / Accepted: 11 October 2019

Abstract

Urchin-like CuS was grown on xanthan gum-derived carbon nanofibers to obtain a sensor for enzyme-free electrochemical sensing of glucose. The unique nanostructure of the sensor provides a large specific surface, more electrocatalytically active sites, and high electrical conductivity. The voltammetric response to glucose, best measured at around 57 mV (vs. Ag/AgCl (E/V)) in 0.1 M NaOH solution, covers two linear ranges, one from 0.1–125 μM, another from 0.16 to 1.2 mM. The sensitivity is quite high (23.7 μA mM^{-1} cm^{-2}), and the detection limit is low (19 nM at $S/N = 3$). The sensor has high selectivity against potentially interfering molecules such as fructose, appreciable operational stability, excellent durability, and good repeatability (with relative standard deviations of 2.3%). It was successfully applied to the determination of glucose in diluted serum samples.

Keywords Xanthan gum derived carbon · Copper sulfide · Electrochemical detection · Enzyme-free biosensor · Human blood serum

Introduction

Insulin is an important contributor that plays a central role in the regulation of both fasting glucose level and glucose tolerance. Therefore, it is necessary to monitor the insulin secretion in physiological fitness. Also the timing achievement of the accurate diagnosis of glucose will contributes to the reduce treatment and to follow strict diabetes management. Thus, the beneficial to accurately or partially minimizing the cause of several diabetic disease or lead to fatal. Simultaneously, developing a rapid and sensitive tool for determination of glucose is a challenge [1]. Electrochemical detection of glucose had a most attractive due to their advantages of fast signal, low cost, easy operation and super sensitivity. There are two types of electrochemical detection of glucose as follows. At first, the enzyme based sensing of glucose has been employed by immobilizing the glucose oxidase on the electrode surface [2]. However, the enzyme based glucose sensors are exhibits good sensitive, but their drawbacks such as high commercial price, the mobility of enzyme, instability in pH variation, and short life time are obstacles the economical plausibility [3]. On the other hand, the application of GOx-based glucose sensor has still shortcomings, including the hindrance of drawbacks like enzyme purification, immobilization and its protection from denaturing [4, 5]. Second, the enzyme-free based sensing of glucose as a rapid, sensitivity and effective to provide a great opportunity due to ease of operation, cost effective, and especially fantastic stability [6, 7]. Based on this, it could be concluded that the non-enzymatic electrochemical sensors are appropriate for glucose detection, which may provide effective in the clinical purpose. Therefore, it is challenge to modify electrode with effective materials in the electrochemical field. So far, the Copper-based materials such as CuO [1], Cu_2O [8] and CuS [9] have been demonstrated as fabricating

Electronic supplementary material The online version of this article (https://doi.org/10.1007/s00604-019-3915-6) contains supplementary material, which is available to authorized users.

✉ Shen-Ming Chen
smchen78@ms15.hinet.net

[1] Department of Chemical Engineering and Biotechnology, National Taipei University of Technology, No. 1, Section 3, Chung-Hsiao East Road, Taipei 106, Taiwan, Republic of China

[2] Institute of Organic and Polymeric Materials and Research and Development Center for Smart Textile Technology, National Taipei University of Technology, Taipei, Taiwan, Republic of China

Published online: 19 November 2019

glucose sensor due to its high catalytic activity, cost-effective, and non-toxicity. Among these, copper sulfide (CuS) with excellent electrochemical performances have been intensively researched and applied in various applications such as sensors, Li-ion batteries, Photocatalyst, solar cell devices and supercapacitors because of its excellent optical, electronic, and other physical properties. Despite, several benefits of CuS, the low electrical conductivity, poor dispersion in solution, and low electron transfer property, significantly limited their effective catalytic contribution. For the purpose of enhancing the electrical conductivity of CuS, several efforts have been undertaken for the preparation of composite with carbon-based materials (CBMs). Nowadays, utilizing CBMs such as graphene, carbon nanotubes, activated carbon, and carbon nanofiber to fabricate highly conductive metal sulfide−carbon hybrid matrices for developing sensor platforms have been increased [10]. These CBMs host of intriguing properties such as superior electrical conductivity, large specific surface area, excellent mechanical strength, and chemical inertness [11]. However, disadvantages such as complicated preparation method and high production cost at a low yield ultimately resulted in casing research on renewable and sustainable carbon materials. Perceptively, carbon materials those derived from small biomolecules such as glucose [12], cellulose [13], guar gum [14] and peach gum [15] etc. have fascinated research attention owing to its commercial availability, cost-effective, renewability, and eco-friendly characteristics. They are produced by many organisms such as plants, animals, fungi, algae, and microorganisms as storage polymers and structure forming macromolecules. These natural small biomolecules with an enormous structural diversity utilized in electrochemical application because of their large surface area, excellent electrical conductivity, and exceptional electrical stability [16].

Xanthan gum (XG) is a polysaccharide, produced by *Xanthomonas campestris* bacteria, which is self-possessed pentasaccharide repeating unit of glucose, mannose, and glucuronic acid [17]. It is widely used in many industries and biomedical applications such as food additive, food packaging, cosmetics, and drug delivery because of their biocompatibility, biodegradability, and biomimetic physicochemical properties [18, 19]. XG exhibit strong binding properties with water and other organic/inorganic materials and they have a number of unique physical and chemical properties [20]. Nevertheless, there have been only a couple of studies reported on the application of XG in fields of biomedicine [21], water treatment [22], as well as the food and beverage industry [23]. To our best knowledge, there is no report on utilizing XG to prepare carbon materials. Herein, the Xanthan gum carbon nanofibers (XGCNFs) was successfully produced using crude biomass small molecule XG as the carbon source via adopted hydrothermal carbonization method for the first time.

A single step hydrothermal method was utilized to synthesize biocompatible CuS/XGCNFs hybrid material by using XG as both carbon source and reaction template and L-cysteine act as both sulfur source and strong reducing agent. The CuS/XGCNFs hybrid material, thereby aiming at improving electrocatalytic activity towards glucose sensing.

Experimental section

Reagents and materials

Copper(II) nitrate trihydrate ($Cu(NO_3)_2.3H_2O$), Xanthan gum (XG), L-cysteine (97%), and glucose (GLU, > 99.5%) were purchased from Sigma-Aldrich (https://www.sigmaaldrich.com/taiwan.html). Here, sodium hydroxide (NaOH) solution (0.1 M) was utilized as a supporting electrolyte for the investigation. All solutions were made throughout the experiment with double deionized water (DI). The human blood serum was purchased from Chang Gung University (CGU) and the experimental strategies were implemented based on the laws and protocols authorized by the committee of CGU, Taiwan.

Characterization techniques

The surface morphology of the CuS nano-flakes and CuS/XGCNFs was taken by the High resolution-transmission electron microscopy (HR-TEM) H-7600, Hitachi, (Japan). The chemical composition and elemental percentage of the materials were assessed through energy-dispersive X-ray (EDX) which affiliated with HR-TEM. The Crystalline nature of the CuS nano-flakes and CuS/XGCNFs was collected in an X-ray diffraction (XRD) XPERT-PRO (PAN analytical B.V. The Netherlands) diffractometer with Cu Kα radiation (k = 1.54 Å). The Raman spectrum of CuS/XGCNFs was recorded using RENISHAW Micro-Raman spectrometer through 514.4 nm He/Ne laser. Brunauer-Emmett-Teller (BET) analysis was executed on the Micromeritics ASAP 2020 M 9 instrument. The oxidation state and composition of the CuS/XGCNFs was scrutinized by Thermo ESCALAB 250 instrument X-ray photoelectron spectroscopy XPS.

Electrochemical techniques

The conventional three-electrode system was utilized with a screen printed carbon electrode (SPCE) and an Ag/AgCl electrode as the working and reference electrodes. A Pt wire electrode as the counter, respectively, were employed for the electrochemical performance. The electrochemical analysis implemented on an electrochemical analyzer CHI 1205b and amperometric, i-t. Electrochemical impedance spectroscopy (EIS) (IM6ex ZAHNER, Kroanch instrument), Germany. To prepare modified SPCE, CuS/XGCNFs (5.0 mg) was

dispersed in DI (1 mL) and kept sonicated for 2 h. Then, 6.0 μL of CuS/XGCNFs was dropped onto SPCE and dried in an air oven for 25 min.

Synthesis of CuS/XGCNF hybrid nanocomposite

The CuS/XGCNFs Hybrid nanocomposite was synthesized by a single-step hydrothermal process. In a typical synthesis method, 1.4 g of L-cysteine and 1.87 g of $Cu(NO_3)_2.3H_2O$ were dissolved in DI water (50 mL) and stirred for 30 min, followed by 0.22 g of XG was added to the above mixture and stirred for 2 h under 35 °C. The final mixture was poured into the 100 mL Teflon lined, stainless steel autoclave, which underwent treatment at 180 °C for 24 h to carry out the reaction. Once the reaction was complete, allowed the autoclave to attain the room temperature. The synthesized final material was collected by centrifugation (6000 rpm) and wash thoroughly with DI and ethanol. Finally, the CuS/XGCNFs material redispersed in ethanol by sonication for 10 min. For comparison, pristine CuS (using 1.4 g of L-cysteine and 1.87 g of $Cu(NO_3)_2$. $3H_2O$ was also synthesized by the same method without adding XG.

Results and discussion

Choice of material

Herein, $Cu(NO_3)_2.3H_2O$ act as the Cu source and L-cysteine act as the dual role of sulfur donor and cross-linker. Xanthene gum (XG) plays multiple roles of the intercalating agent, reaction template, surfactant, and carbon source. The major reason for selecting the XG and L-cysteine as the carbon and sulfur source based on the following considerations. The both XG and L-cysteine, are eco-safe and environmentally sustainable bimolecular materials, can be naturally polymerized under suitable physical-chemical conditions. Owing to its structural diversity and morphology controllable characteristics of XG serve as an excellent reaction template for the formation of the nanocomposite.

Material characterizations

The typical synthetic procedure for the fabrication of urchin-like CuS/XGCNFs from the mixture of $Cu(NO_3)_2.3H_2O$, L-cysteine, and XG is illustrated in Schemes 1 and 2. In the first step, the formation mechanism of pristine CuS flakes is elucidated considering the Cu ion with novel biomolecule precursor L-cysteine, presented in Scheme 1. L-cysteine is a salient biomolecule that contains three reactive functional groups: a carboxylic group (COOH), a thiol (-SH), and an amine (NH_2) group. After adding a copper precursor with L-cysteine solution, creation of stable Copper-L-cysteine complex (Cu^I (μ_2-SH-cysteine)) occurs at pH 7 by the reaction of Cu (II) ion and high affinity –SH group present in the L-cysteine. During autoclaving at ~ 180 °C for 24 h, the Cu^I (μ_2-SH-cysteine complex shattered, and a precise volume of S^{2-} ions are unconfined upon breaking of C-S and S-H bond of L-cysteine. Consequently, S^{2-} ions react with Cu ion and form CuS nuclei which self-aggregated to reduce the surface energy and thus form CuS nano-flakes (CuS NFs) (as presented in Fig. 1a). Intriguingly, the formation of NFs is not much observed in the case of CuS/XGCNFs and the CuS particles are in robust interfacial behavior with XG derived carbon urchins. The deprivation of flake-morphology of CuS in the existence of XG can be deliberated considering the following facts; (1) L-cysteine and $Cu(NO_3)_2.3H_2O$ was dissolved in a certain amount of DI water to form a solution containing Cu^I (μ_2-SH-cysteine) complex. Then, the anionic XG source was added to the above reaction mixture; on the other hand, the amino group of Cu^I (μ_2-SH-cysteine) complex can be absorbed on the XG macromolecular chains backbone through electrostatic interaction ($-NH_3^+\cdots COO^-$). (2) During the hydrothermal treatment, the amine ($-NH_2$) functional groups of Cu^I (μ_2-SH-cysteine) complex can be reacted with the carboxylic reactive groups of XG to form an amide bond. (3) The Maillard chemical reaction and Amadori rearrangement may occur between the oxygen functional groups of XG and amine functional groups of Cu^I (μ_2-SH-cysteine) complex. (4) In the ensuing hydrothermal treatment process, the amide bonded macromolecular chains are converted into carbon. Concomitantly, the copper ions present in the macromolecular chains interact with S^{2-} ion released by L-cysteine to form CuS nuclei and grow in situ on the surface to form urchins self-assembled from CuS NFs [24, 25].

The morphology and nanostructure of the CuS NFs and CuS/XGCNFs were characterized using HR-TEM technique. Figure 1a and b presents the HR-TEM images of CuS NFs at different magnification.

It is observed that the synthetic CuS display dark strips encircled with thin-layer plates. The CuS flakes are 30–40 nm in diameter. In contrast, the HR-TEM images of CuS/XGCNFs presented in Fig. 1c–e, suggest that it has an urchin like nanostructures connected with XGCNFs. The CuS urchins formed by self-aggregation/assembly of thin-layer CuS NFs are tightly connected and anchored on the XG derived CNFs. The diameter of each CuS nano-urchin is calculated to be approximately 500 nm. From the above HR-TEM observations, it can be discerned that the introduction of XG plays a key role in the morphology creation of the CuS/XGCNFs owing to the robust interaction between XG molecular chains containing anionic oxygen functional groups and positively charged Cu^I (μ_2-SH-cysteine) complex. Hence, it is reasonable to conclude that the oxygen functional groups containing XG molecular chains act as multiple roles of soft template, intercalating agent, and surfactant during the hydrothermal

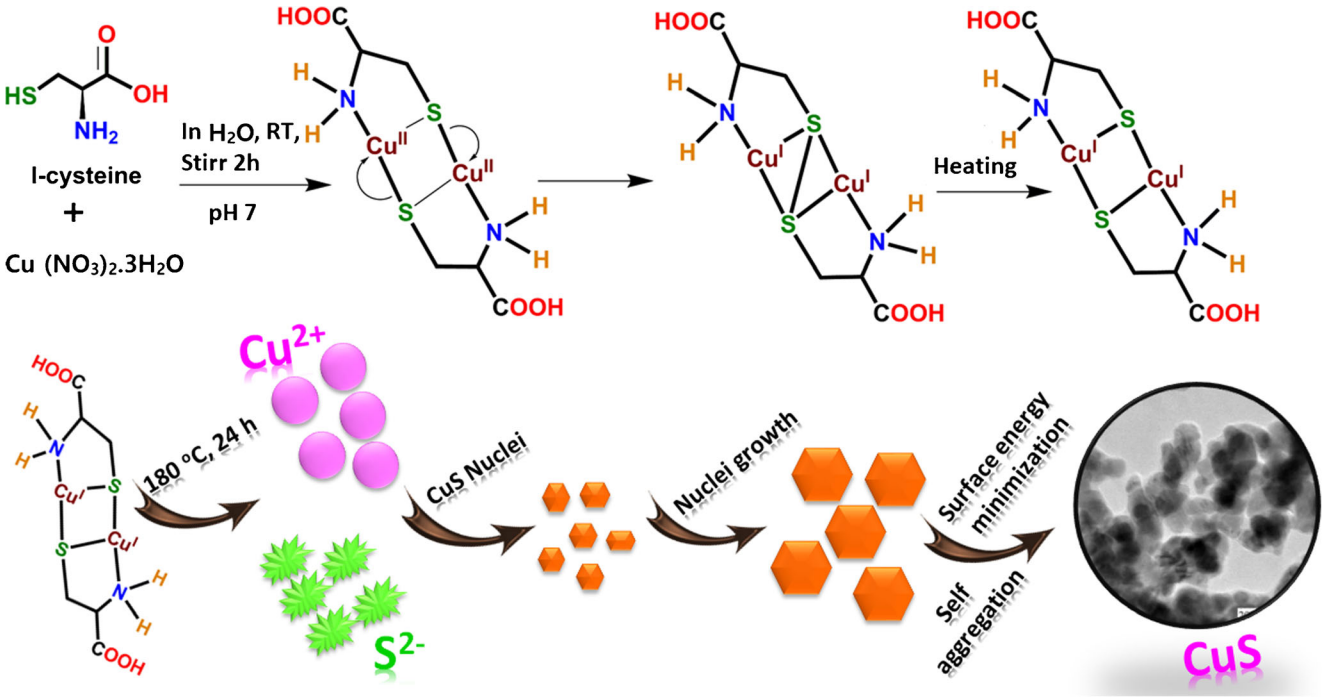

Scheme 1 Schematic illustration of the synthesis mechanism of CuS nanofibers (NFs)

treatment process and effectually altered the growth of CuS nuclei and morphology. Therefore, the particular unique architecture of CuS/XGCNFs is anticipated that improve the active sites and electrochemical performance towards glucose sensing. Additionally, energy dispersive X-ray (EDX) analysis (Fig. S1) demonstrate the presence of copper (Cu), carbon (C), and sulfur (S) in CuS/XGCNFs. EDX were additionally validated by elemental mapping as shown in Fig. 1f. The elemental mappings plainly designate the existence of Cu, C, and S elements with evenly distributed on the CuS/XGCNFs structure.

The crystalline nature of CuS NFs and the CuS/XGCNFs hybrid nanocomposite was further analyzed by the powder XRD patterns, which are shown in Fig. 2a. Major diffraction

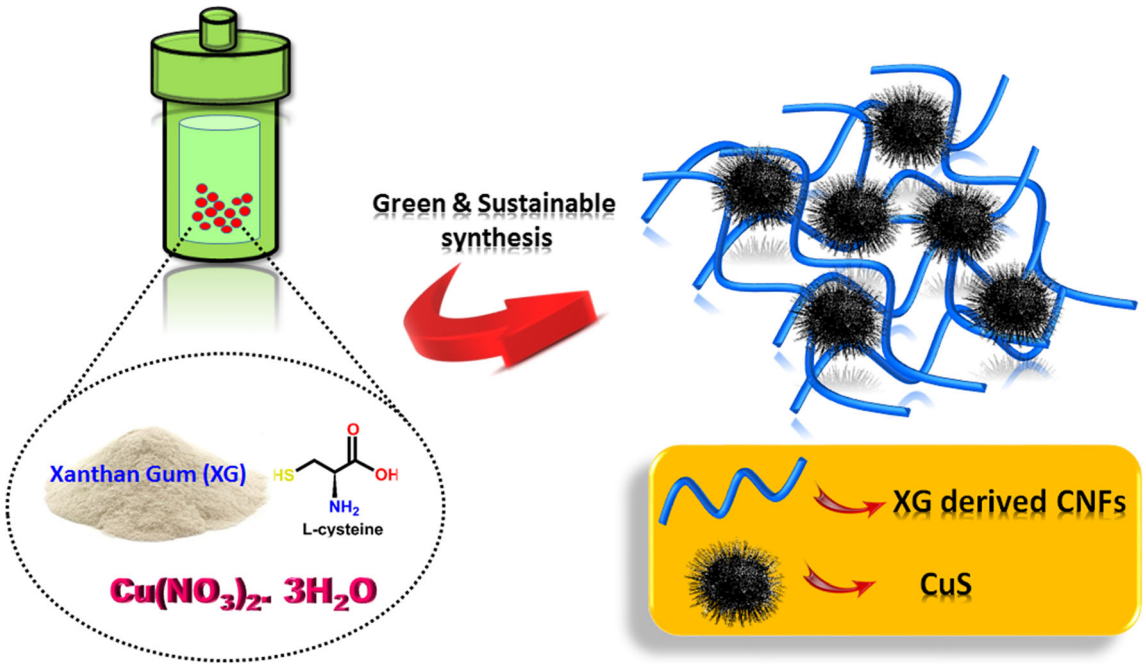

Scheme 2 Schematic representation for the synthesis of CuS/XGCNFs composite

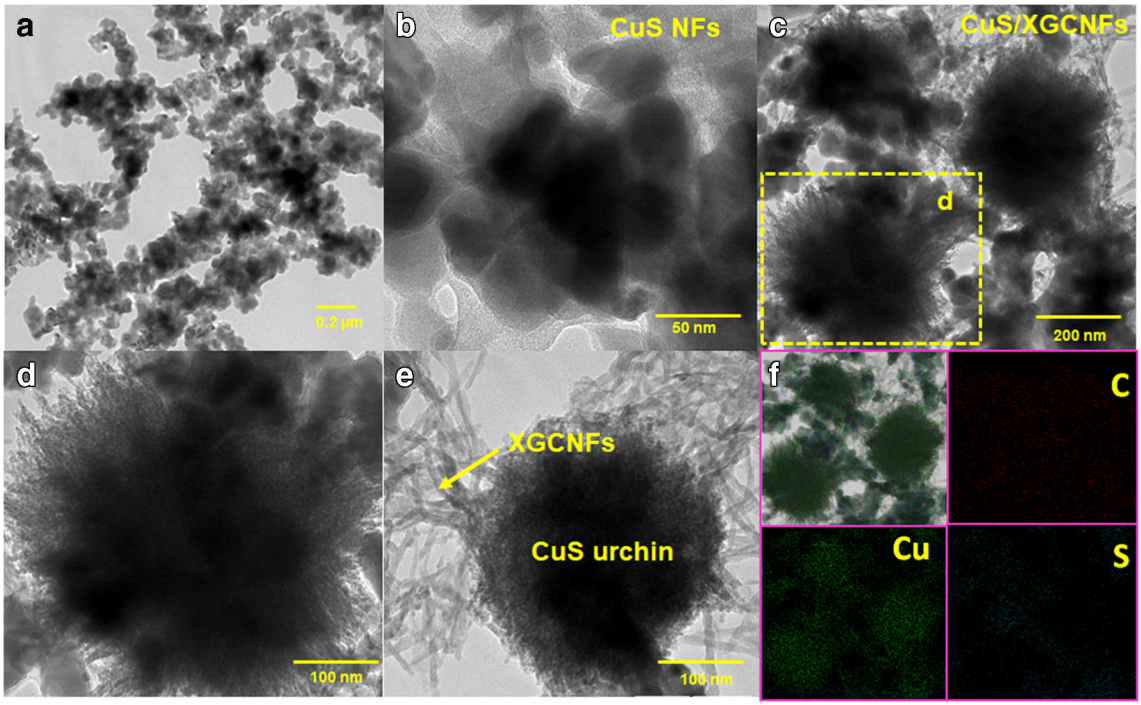

Fig. 1 **a** and **b** HR-TEM images of pure CuS NFs, **c**–**f** CuS/XGCNFs. (Insert in Fig. **f**) The corresponding FFT image, **g** SAED pattern. **h** Elemental mapping of the CuS/XGCNFs

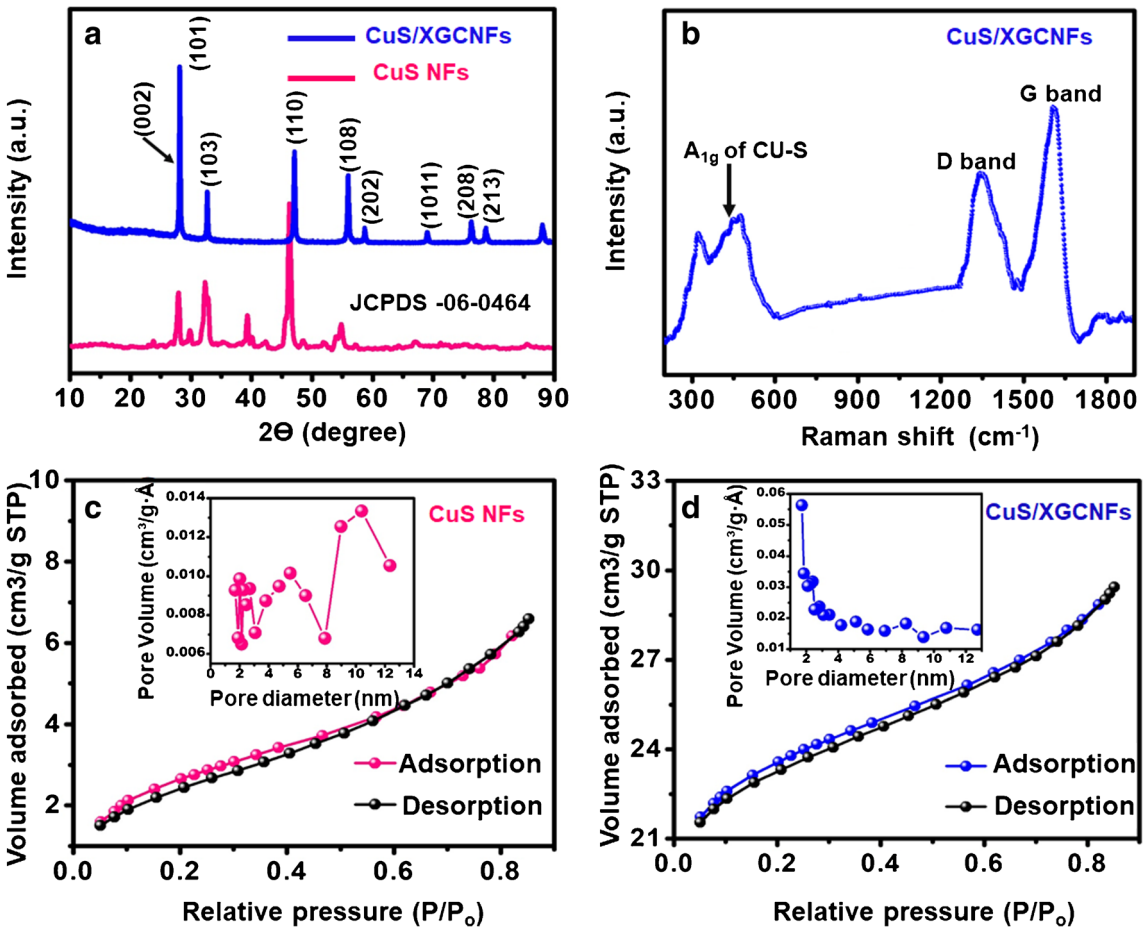

Fig. 2 **a** XRD patterns of CuS NFs and CuS/XGCNFs. **b** Raman spectrum of CuS/XGCNFs. Nitrogen adsorption-desorption isotherm and pore-size distribution (insert) of pristine **c** CuS and **d** CuS/XGCNFs

peaks of the CuS/XGCNFs were found at 2θ = 28.21°, 32.71°, 46.64°, 55.71°, 58.82°, 69.11°, 76.8°, and 79.12° corresponding to the (101), (103), (110), (108), (202), (1011), (208), and (213), crystallographic planes of CuS, which are also present in CuS NFs. However, in the presence of XGCNFs, the CuS shows higher intensity in XRD peaks due to the formation of the perfect crystallographic structure compared to the CuS NFs. The diffraction pattern matches with the standard JCPDS Card No# 06–0464 of CuS and which is also in good agreement with previous reports [26]. A sharp and high intensity peak observed at 2θ = 27.34° in the XRD pattern of the CuS/XGCNFs, which is due to the characteristic peak of graphitic carbon of XGCNFs corresponds to the (002) plane, overlapped with the (101) plane of CuS, indicates strongly attached with CuS in the hybrid nanocomposite. The perfect crystallographic structure of the sample is beneficial for the charge transfer process during glucose sensing.

Raman spectroscopy is a significant technique to understand the structural arrangement of carbon-based hybrid materials. The pure CuS NFs and CuS/XGCNFs hybrid analyzed by Raman spectra as shown in Fig. 2b. Raman spectra of CuS/XGCNFs hybrid clearly exhibits two signature bands of a carbon system, such as G band at 1608 cm^{-1} stretching of sp^2 hybridized carbon atoms and D band at 1346 cm^{-1} that corresponds to the disordered carbon atoms and defects. Whereas, the characteristic peak of CuS at 472 cm^{-1} presented in the spectrum due to strong vibration mode of Cu-S bond, further confirming the successful formation of the hybrid materials.

N_2 adsorption-desorption isotherm analysis was performed to study the BET specific surface area (S_{BET}) and pore structure of the CuS NFs and CuS/XGCNFs (Fig. 2c and d). The hysteresis loop of the sample shows type IV, which are typical characteristics of mesoporous materials according to the IUPAC. The corresponding pore size distribution plot for the CuS NFs and CuS/XGCNFs are presented in the insert Fig. 2c and d. As observed from the experiment CuS NFs has very lower specific surface area of 10.056 $m^2\ g^{-1}$. However, after incorporation of the XGCNFs, specific surface area was increased to 74.057 $m^2\ g^{-1}$ for CuS/XGCNFs, which is 7 fold higher than that of CuS NFs. The larger specific surface area provides more catalytic sites in the CuS/XGCNFs hybrid architecture which favorable for the adsorbing of more glucose molecules through its mesoporous structure resulting in the significant improvement in the electrochemical performance.

The elemental composition and electronic structure of the individual elements in the CuS/XGCNFs were analyzed by XPS (Fig. 3). The presence of Cu (around 935 eV), S (around 165 eV), and C (around 285 eV) further confirmed from the wide range XPS survey spectrum (Fig. 3a). As shown in Fig. 3b, the core level XPS spectra of Cu 2p shows two binding energy at ~933.1 eV and 953.2 eV corresponds to Cu $2p_{3/2}$ and Cu $2p_{1/2}$, respectively, which represents that the Cu^{2+} state. In the high-resolution S 2p spectrum (Fig. 3c), S $2p_{3/2}$ peak observed at ~163.4 eV and S $2p_{1/2}$ peak observed at 164.0 eV can be attributed to the S^{2-} state, revealing the formation of CuS, whereas, another small peak was observed at 168.2 eV, which is aroused from the sulfate molecules. The high-resolution spectra of C 1 s (Fig. 3d) exhibit a high-intensity peak at 285 eV corresponding to C=C/C-C bond and two comparatively weak peaks at 287.2 eV, and 289.5 eV corresponding to C-O and O=C-O bond respectively. The interaction of oxygen atom to the carbon may be aroused from the atmosphere.

Electrochemical impedance spectrum

EIS is frequently utilized as a tool to evaluate the electron transfer ability of the materials.

According to the charge transfer resistance (R_{ct}) of different electrodes, we can receive interfacial impedance change of various electrodes, which corresponds to the interfacial properties. Fig. 4a displays the Nyquist plots of Bare SPCE, CuS SPCE, and CuS/XGCNFs/SPCE in 5 mM $Fe(CN)_6^{3-/4-}$ with the 0.5 M KCl at a frequency range of 1×10^{-1} Hz to 1×10^2 kHz. The R_{ct} value (3 Ω) at CuS/XGCNFs/SPCE is lower than that of Bare SPCE (1839 Ω) and CuS/SPCE (10 Ω), expressing high conductivity and fast electron transfer ability. The synergistic effect between the CuS and XGCNFs, which can accelerate the fast electron transfer kinetics of CuS/XGCNFs/SPCE. Figure 4b shows the comparison plot of R_{ct} vs. different electrodes. It can be clearly observed that the CuS/XGCNFs/SPCE has high electrocatalytic activity than other electrodes.

Electrocatalytic oxidation of GLU

The electrochemical activities of GLU were explored at Bare SPCE, CuS/SPCE, and CuS/XGCNFs/SPCE by cyclic voltammetry (CV). Figure 4c displays the CV curves of Bare SPCE, CuS/SPCE, and CuS/XGCNFs/SPCE in 0.1 M NaOH in the absence and presence of 1 mM GLU at 50 mV/s. The Bare SPCE does not exhibit any significant current (I_{pa} = 1.24 μA) for the detection of glucose owing to inert electron transfer behavior. The slight improvement in the anodic peak current (I_{pa} = 34.78 μA) response of GLU occurred at CuS/SPCE. On the contrary, at CuS/XGCNFs/SPCE, the oxidation peak current density (I_{pa} = 118.88 μA) dramatically enhances with lower positive potential. The observed CV curves exhibit that the oxidation peak currents of GLU on the CuS/XGCNFs/SPCE change from 1.24 μA on the Bare SPCE to 118.88 μA, which indicates that the CuS/XGCNFs/SPCE can provide apparent electrocatalytic activity towards the oxidation of GLU, causing to enhance of the peak current and the decrease of oxidation potential. As compared to Bare SPCE and CuS/SPCE, CuS/XGCNFs/SPCE provides

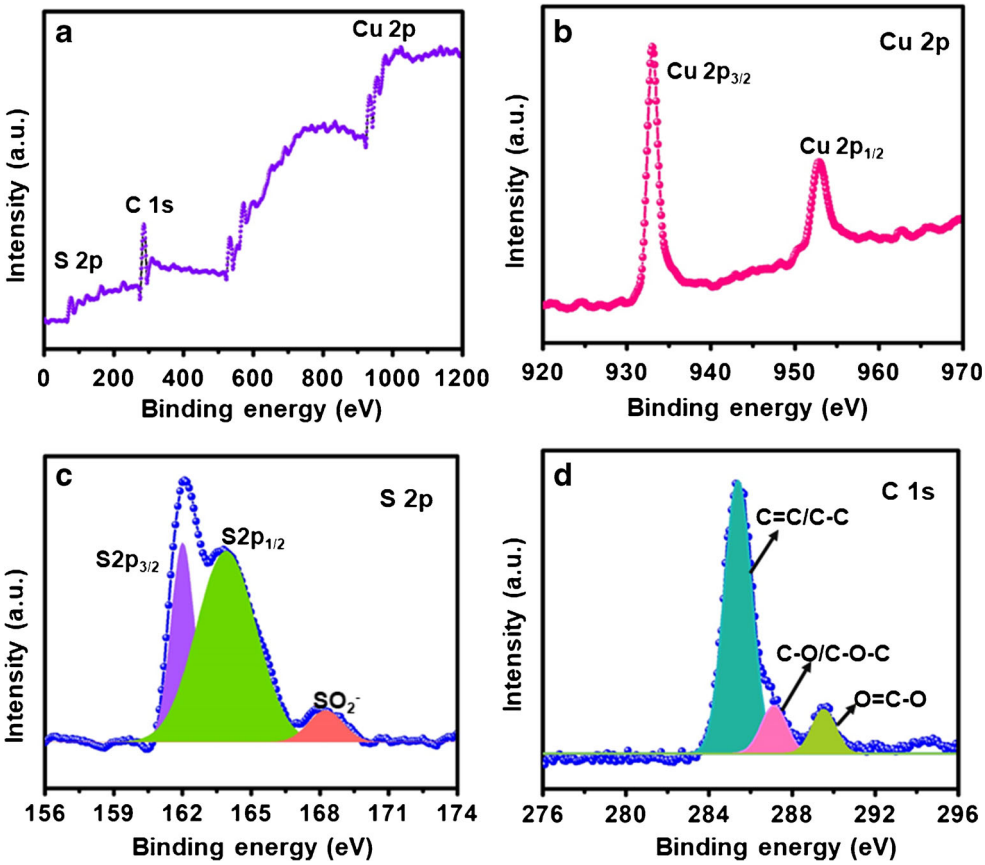

Fig. 3 **a** XPS survey spectra of CuS/XGCNFs. **b**–**d** The high-resolution spectra of Cu 2P, S 2p, and C 1 s of CuS/XGCNFs

a higher electrocatalytic performance on the detection of GLU. Figure 4d shows the calibration plot of GLU current response vs. different electrodes. These results further illustrate that the CuS with XGCNFs has high electrocatalytic activity on GLU sensing owing to their more active sites and high conducting ability. Figure 5a shows the electro-oxidation mechanism of GLU on the CuS/XGCNFs/SPCE in alkaline medium (AM). Thus, the anodic peak for GLU in Fig. 4c is owing to the initial oxidation of CuS can be converted into CuSOH and the copper center grips a highly Cu^{3+} oxidizing state in this system [27]. Further, GLU deprotonation molecule in an AM can initiate isomerization into an enediol structure, which in contact with Cu^{3+} receives oxidized into gluconolactone. Notably, the electrochemical performance of CuS/XGCNFs/SPCE was only investigated in 0.1 M NaOH (alkaline solution), not in any phosphate buffer solution (example: pH 7). It is well known that the strong NaOH solution is etching and a risk to any unskilled person. Although, it has major limitation, some previous reports [4] and our sensor reveals brilliant electrocatalytic activity combined with conductivity, good sensitivity and very low detection limit toward the glucose detection.

To further investigate the electrochemical sensing behavior of CuS/XGCNFs/SPCE on the detection of glucose, we explored the CV response of CuS/XGCNFs/SPCE in 0.1 M NaOH at different concentrations of GLU in the ranges of 0.25–1 mM at 50 mV/s. As shown in Fig. 5b, while raising the concentration of GLU from 0.25–1 mM, the I_{pa} of GLU also increased. The linear regression equation of GLU is found to be I_{pa} (μA) = 120.82 (GLU_{Con}) - 2.94 with a correlation coefficient of 0.9968 (Fig. 5c), which indicates the good electrocatalytic performance of CuS/XGCNFs/SPCE toward the detection of GLU.

To demonstrate the electrochemical process, the influence of the scan rate on the detection of GLU was also studied by CV. The CV of the CuS/XGCNFs/SPCE at various scan rates were ranges of 10–100 mV/s in 0.1 M NaOH containing 1 mM of GLU and the results are shown in Fig. 5d. The curve exhibits a consecutive increase in the oxidation peak current (I_{pa}) with raising in the scan rate ranges of 10–100 mV/s (Fig. 5e). The I_{pa} of GLU is linear with the scan rate, the linear regression equation of GLU is I_{pa} (μA) = 0.689 ( ) + 76.059, which demonstrates an electrooxidation of GLU at CuS/XGCNFs/SPCE was typically the surface-controlled process.

Amperometric response of GLU at CuS/XGCNFs modified electrode

The typical static amperometric response of the CuS/XGCNFs modified electrode towards the consecutive

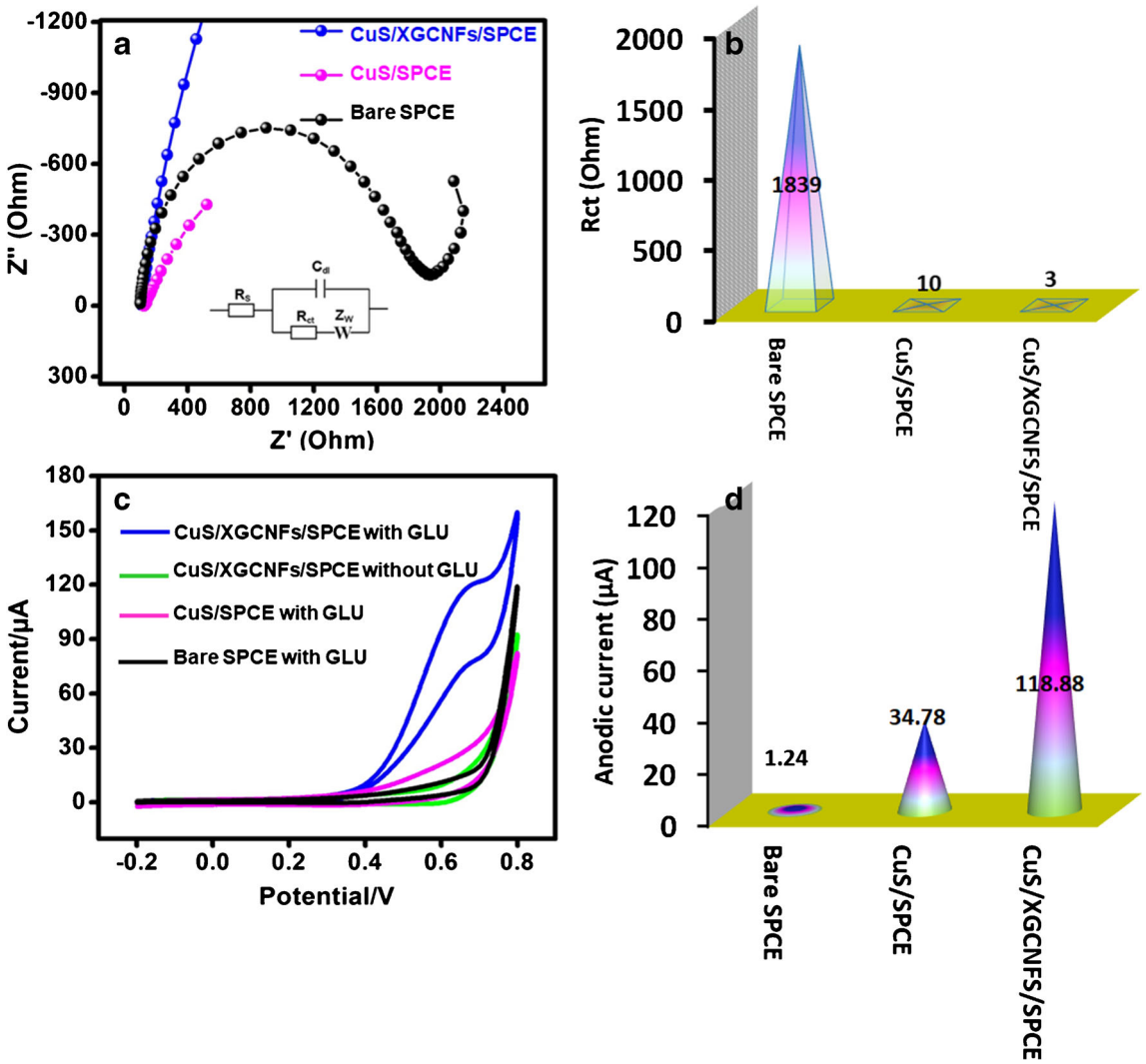

Fig. 4 **a** EIS plots of $Fe(CN)_6^{3-/4-}$ (5 mM containing 0.5 M KCl) at Bare SPCE, CuS/SPCE, and CuS/XGCNFs/SPCE at 1 × 10–1 Hz to 1 × 10^2 kHz. Insert: Randles circuit diagram. **b** The corresponding calibration plot of R_{ct} (Ohm) vs. different electrodes. **c** CV response of SPCEs in 1 mM GLU in 0.1 M NaOH at 50 mV/s. **d** The corresponding calibration plot of anodic current response of GLU (μA) vs. different electrodes

injection of GLU was demonstrated in 0.1 M NaOH with an operating potential of +0.57 V and is shown in Fig. 6a. The steady state current of the CuS/XGCNFs modified electrode can accomplish within 3 s, illustrate the superior electrocatalytic activity of CuS/XGCNFs on the detection of GLU. Figure 6b exhibits the linear plot of current vs. concentration of GLU in the two linear ranges of 0.0001–0.125 mM and 0.158–1.221 mM and the linear regression equations can be calculated as I_{pa} (μA) = 0.4975 GLU_{con} + 6.682 and I_{pa} (μA) = 0.1339 GLU_{con} + 57.857. Further, the limit of detection (LOD; S/*N* = 3) and the sensitivity was evaluated based on the slope value of the linear plot and it was found to be 0.019 μM and 23.69 μA $μM^{-1}$ cm^{-2}, respectively. Table 1 displays the analytical characteristics such as wide linear range, LOD and sensitivity of Cu based non-enzymatic GLU electrochemical sensors in the past few years and it shows that the sensitivity of CuS/XGCNFs modified electrode is higher than other reported sensors due to the more active sites, high conductivity, and synergistic effect of CuS and XGCNFs towards the GLU.

Selectivity, stability, and repeatability studies

The selectivity is also a crucial metrics to estimate the electrochemical sensor performance and thus some possible

Fig. 5 **a** Electrochemical mechanism involved in the oxidation of GLU at different SPCEs. **b** CV response of CuS/XGCNFs/SPCE with various concentrations were ranges of 0.25 mM - 1 mM at 50 mV/s. **c** The linear plot of current vs. concentration of GLU. (d) CV scans of different scan rate (10–100 mV/s) of CuS/XGCNFs/SPCE in 1 mM GLU containing 0.1 M NaOH solution. **e** The calibration plot of current vs. scan rate

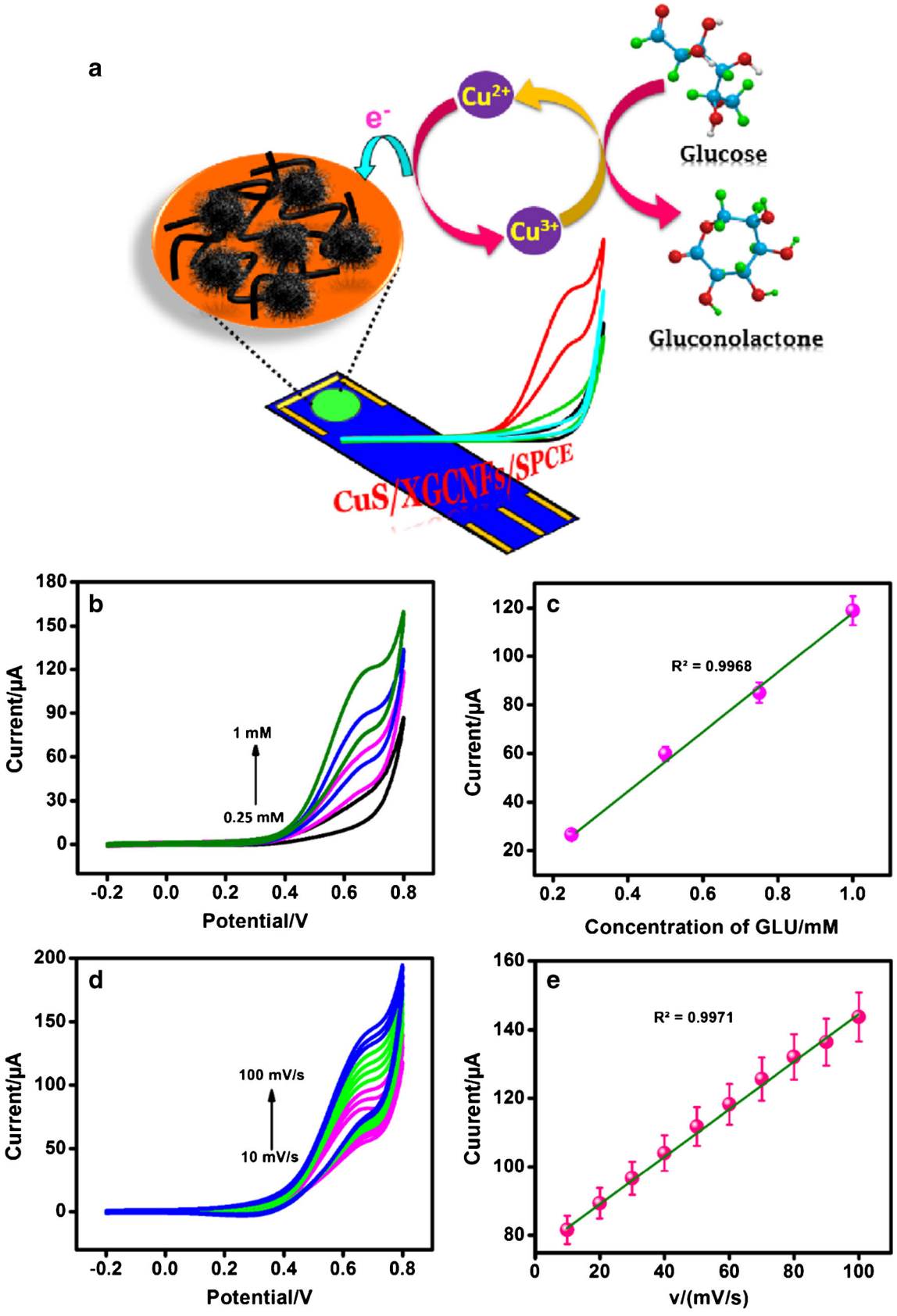
a
e⁻
Cu2+
Cu3+
Glucose
Gluconolactone
CuS/XGCNFs/SPCE
b
Current/μA
1 mM
0.25 mM
Potential/V
c
R² = 0.9968
Current/μA
Concentration of GLU/mM
d
100 mV/s
10 mV/s
Current/μA
Potential/V
e
R² = 0.9971
Cuurent/μA
v/(mV/s)

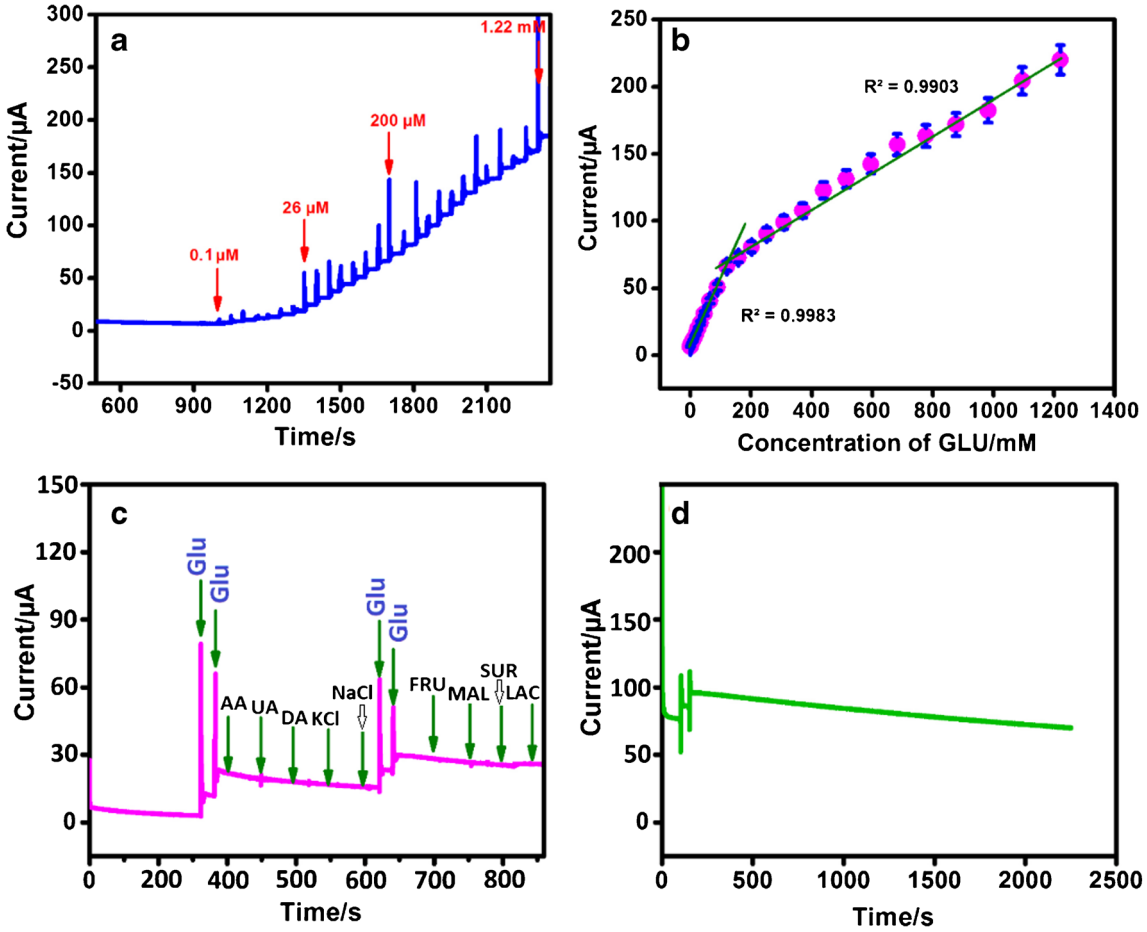

Fig. 6 **a** Amperometric response of CuS/XGCNFs modified electrode upon the consecutive injection of different concentration of GLU in the two linear ranges of 0.0001–0.125 mM and 0.158–1.221 mM at +0.57 V vs. Ag/AgCl. **b** The corresponding linear plot of current vs. concentration of GLU. **c** Amperometric response of interference study of CuS/XGCNFs modified electrode with the consecutive addition of interfering compounds (AA, DA, UA, KCl, NaCl, FRU, MAL, SUR, and LAC) and 0.5 mM GLU in 0.1 M NaOH solution. **d** Stability study of CuS/XGCNFs modified electrode in 0.5 mM GLU containing 0.1 M NaOH

interfering compounds towards the response of GLU were evaluated. Figure 6c displays the amperometric curves of CuS/XGCNFs modified electrode for the successive injection of 0.5 mM of GLU, 0.1 mM ascorbic acid (AA), 0.1 mM dopamine (DA), 0.1 mM uric acid (UA), 0.2 mM KCl, 0.2 mM NaCl, and 0.5 mM GLU. Further, the selectivity of the CuS/XGCNFs modified electrode is also investigated with the commonly found reducing sugar such as fructose (FRU),

Table 1 Comparison of CuS/XGCNFs with previously reported Cu Based Enzyme-Free GLU Electrochemical Sensors

Electrodes	Linear range (mM)	LOD (μM)	Sensitivity	Ref.
Cu-Co/ Reduced graphene oxide (RGO)	0.001–0.04	0.15	0.24 mA mM^{-1} cm^{-2}	[2]
CuS/RGO/CuS/Cu	0.001–0.655 0.655–1.055	0.0005	22.67 and 10.54 mA mM^{-1} cm^{-2}	[28]
CuS nanotubes/Cu	0.0002–2.5	0.045	3135 μA mM^{-1} cm^{-2}	[8]
CuS dendrite Nanoflowers	0.001–4.9	0.04	8337 μA mM^{-1} cm^{-2}	[29]
Cu@Cu_2O nanosheets nanowires	0.0007–2.0	0.04	1420 μA mM^{-1} cm^{-2}	[30]
Cu-Ag_2O nanowalls	0.2–3.2	10	298.2 μA mM^{-1} cm^{-2}	[31]
RGO/CuS nanoflakes	0.001 to 2	0.19	53.5 μA mM^{-1} cm^{-2}	[32]
CuS/XGCNFs	0.0001–0.125 and 0.158–1.221	0.019	23.69 μA μM^{-1} cm^{-2}	This work

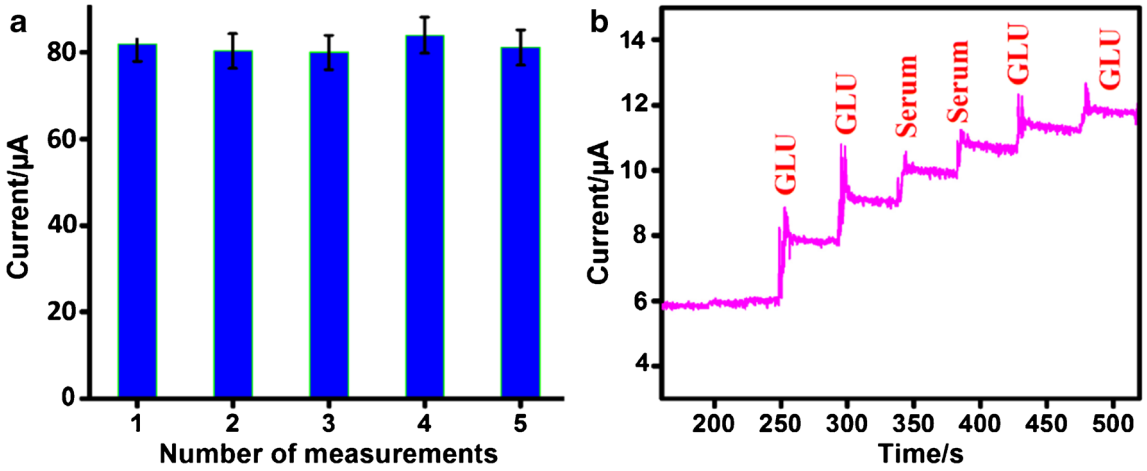

Fig. 7 **a** CV anodic current response of repeatability study of CuS/XGCNFs/SPCE in 0.7 mM GLU with five successive measurements. **b** The amperometric response of CuS/XGCNFs modified electrode upon consecutive additions of GLU (0.1 mM) and human serum sample (10 μM and 15 μM)

maltose (MAL), sucrose (SUR), and lactose (LAC) in blood. It can be clearly seen that the amperometric curves of CuS/XGCNFs modified electrode on the detection of GLU does not influence with the injection of aforesaid interfering species such as AA, DA, UA, KCl, NaCl, FRU, MAL, SUR, and LAC, illustrating the excellent selectivity of CuS/XGCNFs modified electrode for non-enzymatic GLU detection.

The stability of CuS/XGCNFs modified electrode in GLU detection is grasped with its amperometric experiments in 0.5 mM GLU in 0.1 M NaOH at +0.57 V (Fig. 6d). The results indicate that the CuS/XGCNFs modified electrode conserves 92.5% current signal from its amperometric initial current response, meaning its excellent stability. The CuS/XGCNFs/SPCE indicates a relative standard deviation (RSD) of 2.3% for the 5 repeated amperometric measurements in an identical modified SPCE Fig. 7a, demonstrating the superior repeatability of the CuS/XGCNFs/SPCE.

Real sample analysis

The exploration of CuS/XGCNFs modified electrode analytical utility is examined with the amperometric measurements of GLU level in human blood serum samples (HBS). Before the analysis, the HBS was centrifuged and the supernatant was taken for the inspection. Under optimized conditions, the GLU was injected into the diluted serum samples. And also the GLU concentration was estimated with the amperometric response of CuS/XGCNFs modified electrode (Fig. 7b). The recovery results in Table 2 illustrate excellent analytical applicability of this sensor and the corresponding results.

Table 2 Recovery test of the real sample analysis

Sample	Added (μM)	Found (μM)	Recovery (%)
Human blood serum	10	9.8	98
	15	14.9	99.3

Conclusion

We have demonstrated eco-friendly and sustainable synthetic strategy for the preparation of CuS/XGCNFs without using any external reducing and an intercalating agent. The HR-TEM, mapping, XRD, Raman, BET, and XPS studies revealed the formation of hierarchical structure. Interestingly, the synthesized CuS/XGCNFs with unique architecture maximizes the electron transportation, and the aforementioned unique properties of CuS/XGCNFs collectively improve the enzyme-free electrochemical sensing performance towards GLU, which results were successfully demonstrated with the number of electrochemical characterizations. Furthermore, the CuS/XGCNFs sensor exhibits two wide linear range, low detection limit (0.019 μM, $S/N = 3$) with ultrahigh sensitivity, excellent selectivity, good repeatability, and appreciable operational stability. The viability of the CuS/XGCNFs was examined by the determination of GLU in HBS.

Acknowledgements This project was supported by the Ministry of Science and Technology (MOST 106-2113-M-027-003), Taiwan, ROC.

Compliance with ethical standards

Conflict of interest There are no conflicts of interest to declare.

References

1. Bae CW, Toi PT, Kim BY, Lee WI, Lee HB, Hanif A, Lee E.H, Lee NE (2019) Fully stretchable capillary microfluidics-integrated Nanoporous gold electrochemical sensor for wearable continuous

glucose monitoring. ACS Appl Mater Interfaces 11(16): 14567–14575
2. Hu C, Yang DP, Zhu F, Jiang F, Shen S, Zhang J (2014) Enzyme-labeled Pt@ BSA nanocomposite as a facile electrochemical biosensing interface for sensitive glucose determination. ACS Appl Mater Interfaces 6:4170–4178
3. Gao H, Xiao F, Ching CB, Duan H (2011) One-step electrochemical synthesis of PtNi nanoparticle-graphene nanocomposites for nonenzymatic amperometric glucose detection. ACS Appl Mater Interfaces 3:3049–3057
4. Tomanin PP, Cherepanov PV, Besford QA, Christofferson AJ, Amodio A, McConville CF, Yarovsky I, Caruso F, Cavalieri F (2018) Cobalt phosphate nanostructures for non-enzymatic glucose sensing at physiological pH. ACS Appl Mater Interfaces 10:42786–42795
5. Dhara K, Mahapatra DR (2018) Electrochemical nonenzymatic sensing of glucose using advanced nanomaterials. Microchim Acta 185:49
6. Deepalakshmi T, Tran DT, Kim NH, Chong KT, Lee JH (2018) Nitrogen-doped Graphene-encapsulated nickel cobalt nitride as a highly sensitive and selective electrode for glucose and hydrogen peroxide sensing applications. ACS Appl Mater Interfaces 10: 35847–35858
7. Chen X, Liu D, Cao G, Tang Y, Wu C (2019) In situ synthesis of Sandwich-like Graphene@ ZIF-67 Heterostructure for highly sensitive nonenzymatic glucose sensing in human serums. ACS Appl Mater Interfaces 11(9):9374–9384
8. Lin LY, Karakocak BB, Kavadiya S, Soundappan T, Biswas P (2018) A highly sensitive non-enzymatic glucose sensor based on cu/Cu2O/CuO ternary composite hollow spheres prepared in a furnace aerosol reactor. Sensors Actuators B Chem 259:745–752
9. Qian L, Mao J, Tian X, Yuan H, Xiao D (2013) In situ synthesis of CuS nanotubes on cu electrode for sensitive nonenzymatic glucose sensor. Sensors Actuators B Chem 176:952–959
10. Wang S, Han Z, Li Y, Peng R, Feng B (2015) An electrochemical sensor based on reduced graphene oxide and copper sulfide hollow nanospheres. RSC Adv 5:107318–107325
11. Siahrostami S (2018) Designing carbon-based materials for efficient electrochemical reduction of CO_2. Ind Eng Chem Res 58: 879–885
12. De B, Balamurugan J, Kim NH, Lee JH (2017) Enhanced electrochemical and Photocatalytic performance of Core–Shell CuS@carbon quantum dots@carbon hollow Nanospheres. ACS Appl Mater Interfaces 9:2459–2246
13. Elschner T, Heinze T (2015) Cellulose carbonates: a platform for promising biopolymer derivatives with multifunctional capabilities. Macromol Biosci 15:735–746
14. Cheng Y, Pang K, Wu X, Zhang Z, Xu X, Ren J, Huang W, Song R (2018) In situ hydrothermal synthesis MoS2/guar gum carbon Nanoflowers as advanced Electrocatalysts for Electrocatalytic hydrogen evolution. ACS Sustain Chem Eng 6:8688–8696
15. Lin Y, Chen Z, Yu C, Zhong W (2019) Heteroatom-doped Sheet-like and hierarchical porous carbon based on natural biomass small molecule peach gum for high-performance Supercapacitors. ACS Sustain Chem Eng 7:3389–3403
16. Jiang L, Sheng L, Fan Z (2018) Biomass-derived carbon materials with structural diversities and their applications in energy storage. Sci Chin Mater 61:133–158
17. Palaniraj A, Jayaraman V (2011) Production, recovery and applications of xanthan gum by Xanthomonas campestris. J Food Eng 106: 1–12
18. Wang L, Schiraldi DA, Sánchez-Soto M (2014) Foamlike xanthan gum/clay aerogel composites and tailoring properties by blending with agar. Ind Eng Chem Res 53:7680–7687
19. Hamcerencu M, Desbrieres J, Popa M, Riess G (2009) Stimuli-sensitive xanthan derivatives/N-isopropylacrylamide hydrogels: influence of cross-linking agent on interpenetrating polymer network properties. Biomacromolecules 10:1911–1922
20. Ghorai S, Sarkar A, Raoufi M, Panda AB, Schönherr H, Pal S (2014) Enhanced removal of methylene blue and methyl violet dyes from aqueous solution using a nanocomposite of hydrolyzed polyacrylamide grafted xanthan gum and incorporated nanosilica. ACS Appl Mater Interfaces 6:4766–4777
21. Del Agua I, Marina S, Pitsalidis C, Mantione D, Ferro M, Iandolo D, Sanchez-Sanchez A, Malliaras GG, Owens RIM, Mecerreyes D (2018) Conducting polymer scaffolds based on poly (3, 4-ethylenedioxythiophene) and xanthan gum for live-cell monitoring. ACS Omega 3:7424–7431
22. Silva-Medeiros FV, Vernasqui LG, Valderrama P (2016) Xanthan gum as a novel flocculant aid employed in drinking water treatment. Braz J Food Res 7:52–65
23. Andrew T (1979) Application of xanthan gum in food and related products. Extracell Microb Polysaccharide 18:231–241
24. Zhang Y, Tian J, Li H, Wang L, Qin X, Asiri AM, Al-Youbi AO, Sun X (2012) Biomolecule-assisted, environmentally friendly, one-pot synthesis of CuS/reduced graphene oxide nanocomposites with enhanced photocatalytic performance. Langmuir 28:12893–12900
25. Dutta S, Chatterjee S, Mukherjee I, Saha R, Singh BP (2017) Fabrication of ZnS hollow spheres and RGO-ZnS nanocomposite using cysteamine as novel sulfur source: photocatalytic performance on industrial dyes and effluent. Ind Eng Chem Res 56: 4768–4778
26. Zhang J, Feng H, Yang J, Qin Q, Fan H, Wei C, Zheng W (2015) Solvothermal synthesis of three-dimensional hierarchical CuS microspheres from a cu-based ionic liquid precursor for high-performance asymmetric supercapacitors. ACS Appl Mater Interfaces 7:21735–21744
27. Wang P, Gao Y, Li P, Zhang X, Niu H, Zheng Z (2016) Doping Zn^{2+} in CuS Nanoflowers into chemically homogeneous Zn0. 49Cu0. 50S1. 01 Superlattice crystal structure as high-efficiency n-type photoelectric semiconductors. ACS Appl Mater Interfaces 8: 15820–15827
28. Li J, Yan D, Lu T, Qin W, Yao Y, Pan L (2017) Significantly improved sodium-ion storage performance of CuS nanosheets anchored into reduced graphene oxide with ether-based electrolyte. ACS Appl Mater Interfaces 9:2309–2316
29. Kim WB, Lee SH, Cho M, Lee Y (2017) Facile and cost-effective CuS dendrite electrode for non-enzymatic glucose sensor. Sensors Actuators B Chem 249:161–167
30. Zhao Y, Fan L, Zhang Y, Zhao H, Li X, Li Y, Wen L, Yan Z, Huo Z (2015) Hyper-branched cu@Cu_2O coaxial nanowires mesh electrode for ultra-sensitive glucose detection. ACS Appl Mater Interfaces 7:16802–16812
31. Fang B, Gu A, Wang G, Wang W, Feng Y, Zhang C, Zhang X (2009) Silver oxide nanowalls grown on cu substrate as an enzymeless glucose sensor. ACS Appl Mater Interfaces 1:2829–2834
32. Yan X, Gu Y, Li C, Zheng B, Li Y, Zhang T, Zhang Z, Yang M (2018) A non-enzymatic glucose sensor based on the CuS nanoflakes–reduced graphene oxide nanocomposite. Anal Methods 10:381–388